

# Modelling transformation paths of multiphase materials: The triple point of zirconia

Patrick W. Dondl

Max-Planck-Institute for Mathematics  
in the Sciences, Leipzig

Kai Hormann

Department of Informatics  
Clausthal University of Technology

Johannes Zimmer

Department of Mathematical Sciences  
University of Bath

## Abstract

We propose a general method for modelling transformation paths of multi-phase materials such that elastic moduli can be fitted exactly. The energy landscape obtained in this way is global and automatically enjoys the correct symmetries. The method is applied to the triple point of zirconia, where tetragonal, orthorhombic (orthoI), and monoclinic phases meet. An explicit and relatively simple expression yields a phenomenological model in the two-dimensional space spanned by a set of order parameters. We also show how to extend this energy to the apparently first fully three-dimensional model with an exact fit of all given elastic moduli.

## 1 Introduction

We propose a method to derive an explicit phenomenological model of several coexisting stable phases and the relevant transformation paths. The focus is on solid-solid phase transitions. A detailed understanding of the transformation mechanisms is essential both for theory and applications of phase transitions. In theory, the framework of the analysis of solid-solid phase transformations is well established: since diffusion and re-ordering processes are usually negligible, these materials can be well approximated in the realm of nonlinear elasticity. In practice, any constitutive modelling requires an explicit expression for the energy density. It is remarkable that there are very few explicit energy densities available for three space dimensions that interpolate key data such as elastic moduli exactly.

The relative shortage of explicit expressions for energy functions is even more surprising in the light of the subject's long history. The analysis of strain- and temperature-dependent energy functions was initiated by Landau [20]. A more recent line of investigation based on the Cauchy-Born hypothesis in continuum mechanics can be traced back to Ericksen [10]. A common method for deriving energy densities is to expand the energy function in invariant polynomials of lowest order and fit as many degrees of freedom as possible, or to obtain a best fit in some error norm. As for the triple point of zirconia ( $\text{ZrO}_2$ ), when working with an expansion in invariant polynomials, it requires considerable ingenuity to obtain a reasonable or good match of most moduli [11]; not all moduli can be fitted this way, let alone further information of the transformation path. This observation is not surprising given that polynomials offer little flexibility to control the energy along (transformation) paths. It has been observed [14] that the minimal set of order parameters may lead to unrealistically high estimates for the thermal activation energy. Consequently, to determine the energy barrier correctly, non-symmetry-breaking order parameters or, more specifically, invariant polynomials of higher order are employed in [14]. With the advent of *ab initio* calculations, data for the transformation point becomes available, and it is thus reasonable to ask for a method that can provide an exact reproduction of experimental data obtained along the entire transformation path, including data at the stable phases. With regard both to the theory and applications of solid phase transitions, there is a general interest in devising

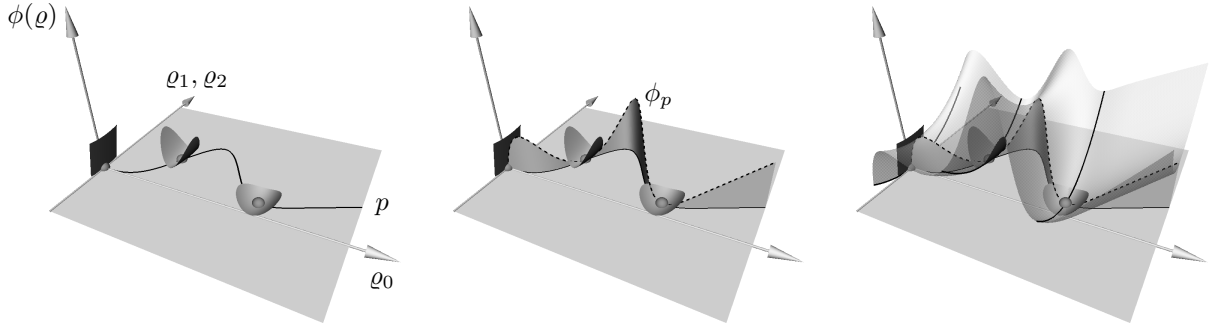


Figure 1: Left: Visualisation of the input data in a space of invariant polynomials of the strain tensor; see Section 2.3. Here, the space of invariant polynomials is visualised as a plane. The stable phases are marked by spheres and the moduli are indicated by quadratic wells around the phases. A transformation *path*  $p$  connecting the stable phases is indicated as a solid line. It is defined in the space of invariant polynomials and parameterised by the order parameter  $\varrho_0$ . Middle: A *profile*  $\phi_p$  (dashed) is defined along the path. Right: The growth away from the path is modelled by a family of *paraboloids*, parameterised by the path so that the given elastic moduli are interpolated.

a methodology that allows for the integration of experimental data for multi-phase materials into the energy density via a straightforward and phenomenological, yet natural approach.

To achieve this aim, we propose an intuitive method. The stable phases are first connected by a *path* that mimics the kinematic transformation path (if measurements are available). The path is modelled in the space of invariant polynomials so that the correct symmetries are automatically ensured. In Figure 1 (left) such a path is visualised for a material with three stable phases. The wells in the figure indicate the respective elastic moduli and  $\varrho_0, \varrho_1, \varrho_2$  are the symmetry-adapted coordinates we employ to deal with the crystalline symmetry (see Section 2.3 below for details). The path is parameterised by a suitable invariant, here  $\varrho_0$ . We remark that in general the symmetry-adapted coordinates may form a collection of manifolds. The framework presented here allows for, under weak assumptions, a reduction of this nonlinear setting to a linear one, without loss of generality. Consequently, the coordinates are visualised as a plane in Figure 1. A *profile* then models the energy along the path and thus has minima at the stable phases and energy barriers in between; see Figure 1 (middle). In addition, we model the growth of the energy away from the path. Here, a quadratic growth is chosen, which is sufficient and keeps the global order low. We first construct at each stable phase a *paraboloid* that interpolates the elastic moduli locally, and then interpolate between them along the path. This interpolation can be interpreted as a continuously deforming paraboloid that slides along the profile curve and blends one locally fitted paraboloid into the next; see Figure 1 (right). A plot of a schematic energy landscape obtained this way is shown in Figure 2. In Section 3 we explain why this *ansatz* gives enough freedom to fit all elastic moduli exactly.

To demonstrate that this approach is capable of fitting available data, we consider zirconia as a case study. This choice is motivated by Gibb’s phase rule, according to which a one-component system can have at most three phases in coexistence, namely at the triple point, which occurs at one specific combination of pressure and temperature. Thus, a triple point is the most complicated scenario for single-component materials. Zirconia has a triple point with tetragonal, orthorhombic (orthoI) and monoclinic phases in coexistence. While the analysis of phase transformations in zirconia is of interest for applications such as toughening of ceramics, the high pressure and temperature at the triple point render experimental investigations difficult. Numerical simulations offer an alternative. Yet, they are currently hampered by a lack of a simple energy function that has minimisers only at experimentally observed phases, and fits available experimental data exactly. We give such an expression in Section 3.3 and present some numerical simulations in Section 4.

For the triple point of zirconia, a simple count of the degrees of freedoms shows that an invariant polynomial of lowest order does not offer enough parameters to match all moduli. Higher-order invariant

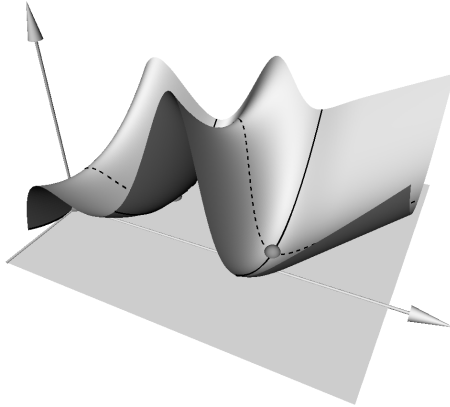


Figure 2: A schematic plot of the final energy landscape.

polynomials provide a theoretical remedy for this problem, but are rarely used in practice. One problem is that the calculations for the derivation become very cumbersome, and it can be hard to verify that higher-order polynomials do not introduce spurious minima. In addition, the steep growth of higher-order polynomials often poses a challenge for simulations. At present, the generic Landau strain-energy function constructed by Truskinovsky and Zanzotto [27] and its augmentation by four new coupling terms to fit experimental data [11] seem to be the best three-dimensional energies for zirconia available. In two space dimensions, an approach using splines is able to match all available moduli exactly [9]. While the path from the tetragonal phase to an orthorhombic minimum for a polynomial energy of lowest order is extremely shallow, splines offer enough flexibility to model a significant energy barrier. Straightforward numerical simulations with a spline energy can capture the corresponding pattern formation, while they fail to do so for a polynomial energy [9]. However, the spline energy in [9] itself involves a finite element simulation and cannot be written down in a simple and concise form; it is also not evident how to extend it to three dimensions.

The energy in [9] is continuously differentiable ( $C^1$ ) and the authors report that no spurious effects stemming from the discontinuity in the elastic moduli were ever observed in numerical studies of boundary value problems. This is in line with other simulations with piecewise defined  $C^1$  energy densities [17]. However, we derive here an energy that is twice continuously differentiable ( $C^2$ ) since the relevant data involves derivatives up to the second order. Moreover, the construction could easily be extended to fit an energy density with an arbitrary degree of smoothness.

The framework proposed in this paper renders the task of fitting parameters a profoundly simple one. This could signify that the construction has a deeper physical significance. Specifically, for a transition characterised by the softening of a modulus (like the tetragonal-orthorhombic transition considered here) the chosen path seems to capture the softening remarkably well. Polynomials, on the other hand, are in general too rigid to accurately model a path determined by a softening direction. Further, a polynomial expansion of the energy for CuAlNi [13] does not match all elastic moduli, while an approach similar to the one advocated here does provide a perfect fit for InTl [16], which, like CuZnAl, can undergo a cubic-to-monoclinic transition. In general, non-polynomial energy densities have been found to be a good approximation for InTl [18].

## 2 Relevant data for zirconia

### 2.1 Transformation paths in zirconia

Zirconia has a triple point near 1.8 GPa and 840 K, where a tetragonal (t), an orthorhombic (o) and a monoclinic (m) phase meet. A quick review of the crystallographic aspects of these phases is included here for the reader's convenience. We choose the tetragonal phase as reference configuration; see Figure 3

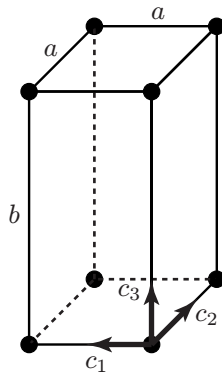


Figure 3: Tetragonal phase with lattice parameters  $a$  and  $b$ ;  $c_1, c_2$  and  $c_3$  denote the axes.

for the relevant primitive tetragonal Bravais lattice. The lattice is spanned by three mutually orthogonal basis vectors  $c_1, c_2$  and  $c_3$ . It is easy to verify that  $R_{c_1}^\pi$  and  $R_{c_3}^{\pi/2}$  generate the tetragonal point group  $T_3$ , where  $R_c^\alpha$  denotes the rotation with angle  $\alpha$  about axis  $c$  (only orientation-preserving symmetry operations are considered in this paper). We restrict the crystallographic discussion to skeletal lattices; a visualisation of the movements of the atoms inside the skeletal lattices is given in [11].

There are two orthorhombic and five monoclinic subgroups and it can be seen that there are four essentially different t-o-m paths [27], going from the tetragonal phase through an orthorhombic to a monoclinic phase. Based on the best-established t-o orientational relationship of the respective axes and the coordination of O atoms with the Zr atoms, a transition path has been suggested [27] which involves the monoclinic group  $M_3 := \{1, R_{c_3}^\pi\}$  generated by  $R_{c_3}^\pi$  and the orthorhombic group  $O_{123} := \{1, R_{c_1}^\pi, R_{c_2}^\pi, R_{c_3}^\pi\}$ . Though alternative kinematic paths for the phase transformations in zirconia have been suggested (e.g., [3, 25]), we follow [27] in considering the transformation mechanism

$$T_3 \rightarrow O_{123} \rightarrow M_3.$$

It is known that the bifurcation associated with the transition  $T_3 \rightarrow O_{123}$  originates from the softening of the tetragonal modulus  $C_{11} - C_{12}$ , while the path  $T_3 \rightarrow M_3$  does not directly correspond to a softening of a tetragonal modulus [11]. This seems natural in the light of the separation of the tetragonal and the monoclinic phases by the orthorhombic phase which makes the  $T_3 \rightarrow M_3$  transition appear as consecutive bifurcation.

The cubic, tetragonal and monoclinic phases of  $\text{ZrO}_2$  have been investigated with lattice dynamics in [19], where the phonon vibrations and the density of states for those phases were determined with the VASP code for ground state calculations combined with the direct method for dynamics.

## 2.2 Coordinates of the stable phases

Let  $y(x)$  denote the deformation at a point  $x$ . The free-energy density per unit reference volume, henceforth energy function for short, is a function of the deformation gradient  $F_{jk} := \frac{\partial y_j}{\partial x_k}$ . By frame indifference, the energy function  $\Phi$  can be written as a function of  $C := F^T F$  or equivalently in terms of the Green-St. Venant strain tensor  $E := \frac{1}{2}(F^T F - \text{Id})$ . In Voigt's notation,

$$E = \begin{pmatrix} e_1 & \frac{1}{2}e_6 & \frac{1}{2}e_5 \\ \frac{1}{2}e_6 & e_2 & \frac{1}{2}e_4 \\ \frac{1}{2}e_5 & \frac{1}{2}e_4 & e_3 \end{pmatrix}$$

with  $e_j \in \mathbb{R}$ ,  $j = 1, \dots, 6$ . The energy  $\Phi = \Phi(e_1, \dots, e_6)$  has to be invariant under the tetragonal point group  $T_3$ .

	tetragonal	orthorhombic	monoclinic
$e_1$	0.0	$9.39046 \cdot 10^{-3}$	$4.68924 \cdot 10^{-2}$
$e_2$	0.0	$-5.39105 \cdot 10^{-3}$	$8.50962 \cdot 10^{-3}$
$e_3$	0.0	$1.71769 \cdot 10^{-2}$	$-5.33516 \cdot 10^{-4}$
$e_4$	0.0	0.0	0.0
$e_5$	0.0	0.0	0.0
$e_6$	0.0	0.0	$-3.28543 \cdot 10^{-1}$

Table 1: The minima in strain space, calculated for 1.8 GPa and 840 K from data for the relevant lattice parameters in the Appendix of [11]. The data is rounded to the 5th digit.

We calculate the position of the t–o–m phases in strain space for 1.8 GPa and 840 K from data for the relevant lattice parameters in [11]. The location of the t-o-m phases in strain space is listed in Table 1.

### 2.3 Symmetry constraints

For the t-o-m transition under consideration, a set of order parameters is given by  $e_1 - e_2$  and  $e_6$ . Since the transition at the triple point can be described in terms of the order parameters only, we first derive an energy in  $e_1$ ,  $e_2$  and  $e_6$  and later augment this energy to an energy that depends on the full strain tensor. Both for the reduced and the full set of strain variables, we first identify a suitable basis (a Hilbert basis, see Section 2.3.1) of polynomials  $\varrho := (\varrho_0, \dots, \varrho_{n-1})$ , where each polynomial depends on the strain variables. We then construct the energy as a function  $\phi(\varrho)$ , and finally the energy in strain space for  $e := (e_1, \dots, e_6)$  is  $\Phi(e) := \phi(\varrho(e))$ .

We remark that the choice of the order parameters involves an assumption; to describe the microscopic deformation of the lattice in a macroscopic manner, we follow the conventional assumption that the Cauchy-Born hypothesis applies; this hypothesis states that the microscopic lattice deforms according to the macroscopic deformation. Since we wish to contrast the method presented here with the polynomial expansion going back to Landau, we follow [11, 27] and consider order parameters which are functions of the strain as described above. Since the transformation can be well described by the deformation of one lattice supercell, this seems appropriate. The analysis of phase transitions that cannot be described in this framework is the topic of a future investigation. Of particular interest in this instance are phase transitions of multi-lattices; then, the relative shift of the lattices can take place in a way which violates the Cauchy-Born hypothesis. Thus, the relevant shift has to be incorporated as additional order parameter in the energy [7]. While this complicates the modelling, the principal ideas laid out in this article essentially extend to the situation in [7].

#### 2.3.1 Invariants for the Landau contribution

The first step in the construction is to incorporate the symmetry constraints of the tetragonal point group. As the order parameters show, the t–o–m symmetry breaking takes place in the  $c_1$ - $c_2$ -plane shown in Figure 3. Thus, we restrict our attention to the corresponding two-dimensional subspace spanned by  $c_1$  and  $c_2$ ; the strain space is then spanned by the three strain variables  $e_1$ ,  $e_2$  and  $e_6$ . For this subspace, the three polynomials

$$\begin{aligned}
\varrho_0(e_1, e_2, e_6) &:= (e_1 - e_2)^2, \\
\varrho_1(e_1, e_2, e_6) &:= e_1 + e_2, \\
\varrho_2(e_1, e_2, e_6) &:= e_6^2
\end{aligned} \tag{1}$$

are invariant under the (restriction of the) tetragonal point group. In addition, these polynomials have the special property that every polynomial  $\tilde{\varrho}$  with this invariance can be written as  $\tilde{\varrho}(e_1, e_2, e_6) = P(\varrho_0, \varrho_1, \varrho_2)$  for some polynomial  $P$ . The mathematical background for this statement is given in [29, 9].

	tetragonal	orthorhombic	monoclinic
$\varrho_0$	0.0	$2.18493 \cdot 10^{-4}$	$1.47324 \cdot 10^{-3}$
$\varrho_1$	0.0	$3.99941 \cdot 10^{-3}$	$5.54020 \cdot 10^{-2}$
$\varrho_2$	0.0	0.0	$1.07941 \cdot 10^{-1}$
$\varrho_3$	0.0	$1.71769 \cdot 10^{-2}$	$-5.33516 \cdot 10^{-4}$

Table 2: The location of the minima in orbit space, calculated for the strain data given in Table 1. The polynomials  $\varrho_4, \dots, \varrho_7$  in (3) as well as  $\varrho_8, \varrho_9$  in (5) vanish at all three phases. The data is rounded to the 5th digit.

In a nutshell, by Hilbert’s Theorem [28], there is a basis  $\varrho_0, \dots, \varrho_{n-1}$  such that every invariant polynomial can be written as a polynomial of the polynomial basis, and by Chevalley’s Theorem [5, Theorem A], there has to be a basis with  $n = 3$  elements for the tetragonal point group. Since the polynomials in (1) are of lowest degree, they form such a basis. For us, it is convenient to introduce invariants in the order parameters  $e_1 - e_2$  and  $e_6$ , which is why the basis chosen here differs from the one in [9].

We observe that any function of the polynomials in (1) automatically enjoys the correct symmetry: points in strain space that are mapped to each other under tetragonal symmetry are mapped by  $\varrho := (\varrho_0, \varrho_1, \varrho_2)$  to the same point, while points that are not symmetry related are mapped to different points by  $\varrho$ . The map  $\varrho$  is, as  $\varrho_0, \varrho_1, \varrho_2$ , a function of the strain; it identifies points in the strain space which are mapped to each other under the symmetry group. The map  $\varrho$  is thus injective on a fundamental domain; one way of visualising  $\varrho$  is to think of it as a function that maps the entire strain space to a suitably deformed fundamental domain. The deformation is such that points on the boundary of the fundamental domain are identified as appropriate. This identification facilitates the definition of the energy, as can be seen in the toy model of the invariance being defined by a rotation about  $\frac{\pi}{2}$  in  $\mathbb{R}^2$ ; any quadrant is a fundamental domain. If one tries to define the energy on a quadrant, then one needs to take into account that points on the boundaries are identified (mapped to each other under the symmetry group) in a pairwise manner. This imposes a constraint on the energy function. The map  $\varrho$  would in this case map the model strain space  $\mathbb{R}^2$  to the surface of a cone obtained by taking the fundamental domain (quadrant) and gluing together the boundaries pointwise (e.g., identifying  $(x, 0)$  with  $(0, x)$  for  $x \in \mathbb{R}$  for the quadrant  $\{(x, y) \mid x > 0, y > 0\}$ ). Thus, the constraint that points have to be identified disappears when the map  $\varrho$  is applied to the strain space, and the definition of the energy function simplifies significantly. The image of the strain space  $\mathbb{R}^3$  under the map  $\varrho$  is called *orbit space*. Any function defined in orbit space automatically exhibits the correct symmetries. Here, the orbit space for the Landau contribution is the quadrant

$$\{(\varrho_0, \varrho_1, \varrho_2) \mid \varrho_0 \geq 0 \text{ and } \varrho_2 \geq 0\} \quad (2)$$

and the position of the stable phases in orbit space is recorded in Table 2.

### 2.3.2 Invariants in the three-dimensional setting

Analogous to the two-dimensional basis in (1), the eight invariant polynomials

$$\begin{aligned}
\varrho_0(e_1, \dots, e_6) &:= (e_1 - e_2)^2, \\
\varrho_1(e_1, \dots, e_6) &:= e_1 + e_2, \\
\varrho_2(e_1, \dots, e_6) &:= e_6^2, \\
\varrho_3(e_1, \dots, e_6) &:= e_3, \\
\varrho_4(e_1, \dots, e_6) &:= e_4^2 + e_5^2, \\
\varrho_5(e_1, \dots, e_6) &:= e_4^2 e_5^2, \\
\varrho_6(e_1, \dots, e_6) &:= e_4 e_5 e_6, \\
\varrho_7(e_1, \dots, e_6) &:= e_1 e_4^2 + e_2 e_5^2
\end{aligned} \quad (3)$$

form a basis in the three-dimensional setting for the full strain tensor with strain variables  $e_1, \dots, e_6$ .

We computed these invariants with the library `finvar.lib` of `Singular` [15]. However, tetragonal invariants can also be read off from the literature [26]. In the three-dimensional setting, we employ the same notation and terminology as introduced for the Landau framework in Section 2.3.1.

We remark that it is also possible to work in symmetry-adapted coordinates, e.g.,  $y_1 := e_1 + e_2 + e_3$  to characterise homogeneous dilations,  $y_2 := \frac{1}{\sqrt{6}}(e_1 + e_2 - 2e_3)$ ,  $y_3 := \frac{1}{\sqrt{2}}(e_1 - e_2)$ ,  $y_j := e_j$  for  $j \in \{4, 5, 6\}$ . This has been done successfully in [11] to simplify the calculations. Yet, in the framework presented here, it is not less convenient to work directly in strain coordinates.

### 3 The path-profile construction

#### 3.1 Concept

The proposed construction relies on three simple ingredients: a *path* in the orbit space to model the kinematic transformation path, a *profile* to model the energy along the path, and a *paraboloid* to model the growth away from the path.

The invariance of the energy will be automatically obtained by deriving the energy in the space of invariants, that is, the image of the strain space under the mapping  $\varrho := (\varrho_0, \dots, \varrho_{n-1})$ ; in the two-dimensional Landau setting, we have  $n = 3$  (see Section 2.3.1), while  $n = 8$  in the full three-dimensional setting (see Section 2.3.2).

The *path* must interpolate all stable phases. Here, we select one order parameter to parameterise the path. Specifically, we work with  $\varrho_0$ , though other choices are possible as well. Since  $\varrho_0$  is an order parameter, its evaluations at the tetragonal, orthorhombic and monoclinic phases are mutually different. The ordering is such that the orthorhombic phase separates the tetragonal phase on the left from the monoclinic phase on the right. We then construct a mapping  $\pi: \mathbb{R} \rightarrow \mathbb{R}^{n-1}$  that interpolates the three phases located at  $\varrho^\star = (\varrho_0^\star, \dots, \varrho_{n-1}^\star)$  for  $\star \in \{t, o, m\}$  in the sense that  $\pi(\varrho_0^\star) = (\varrho_1^\star, \dots, \varrho_{n-1}^\star)$ . Note that the  $n - 1$  components  $\pi_j$  of  $\pi$  can be modelled independently of each other. The path  $p$  can then be seen either as the graph of the function  $\pi$ , that is,  $p := \{(\varrho_0, \pi(\varrho_0)) \mid \varrho_0 \in \mathbb{R}\} \subset \mathbb{R}^n$ , or as the zero-set of the mapping

$$\psi: \mathbb{R}^n \rightarrow \mathbb{R}^{n-1}, \quad \varrho \mapsto (\varrho_i - \pi_i(\varrho_0))_{i=1, \dots, n-1},$$

$p = \{\varrho \in \mathbb{R}^n \mid \psi(\varrho) = (0, \dots, 0)\}$ ; then  $\varrho^t, \varrho^o, \varrho^m \in p$ . This path approximates the kinematic transition path and it would not be difficult to accommodate any explicit knowledge of the transformation path, such as the position of saddle points of the energy. For zirconia, no exact data seems to be available for the kinematic transformation path other than the position of the stable phases; we thus choose a path that simply interpolates between the stable phases. Some care must be taken that the path remains within the orbit space  $\varrho(\mathbb{R}^3)$  for the Landau part, respectively  $\varrho(\mathbb{R}^6)$  in the three-dimensional setting. This is since the orbit space is defined by homogeneous polynomials, which results in a half-space if the degree is even. For example, the orbit space (2) for the Landau contribution in Section 2.3.1 is only a quadrant of  $\mathbb{R}^3$  because  $\varrho_0$  and  $\varrho_2$  are polynomials of even degree.

The *profile* must have global minima at the stable phases, and without loss of generality, we can choose zero as the value there. We remark that the method proposed here is also suited for fitting wells of unequal height, for example for a loading experiment. Let  $\phi_p: \mathbb{R} \rightarrow \mathbb{R}_0^+$  denote the energy along the path. This profile models the energy barriers (that is, saddles in the three-dimensional energy landscape) and the wells along the path  $p$ . Figure 1 (middle panel) shows such a profile construction.

Finally, a *paraboloid* is employed to model the growth of the energy away from the transition path. This choice mirrors the ansatz with invariant polynomials of lowest order. Using quadratic functions for this purpose results in the slowest possible growth of the energy for which the moduli can be fitted, and simultaneously yields the lowest degree functions of the invariants. In order to fit the moduli of elastic phases at the boundary of the orbit space, we need further to introduce a linear contribution in the invariant polynomials of even degree (cf. the linear behaviour in  $\varrho_0$  for the stable phase at the boundary in Figure 1). Together with a properly chosen path and profile, the combination of linear and quadratic contributions allows us to match all prescribed elastic moduli at given phases exactly.

Modulus	tetragonal	orthorhombic	monoclinic
$C_{11}$	340.0	300.0	312.0
$C_{12}$	33.0	33.0	35.2
$C_{13}$	160.0	★	155.0
$C_{16}$			3.2
$C_{22}$	$= C_{11}$	350.0	350.0
$C_{23}$	$= C_{13}$	★	171.0
$C_{26}$			4.3
$C_{33}$	325.0	★	341.0
$C_{36}$			9.4
$C_{44}$	66.0	★	101.0
$C_{45}$			-13.9
$C_{55}$	$= C_{44}$	★	81.6
$C_{66}$	95.0	90.0	66.3

Table 3: Elastic constants of the tetragonal and the monoclinic phase in GPa. Here,  $C_{11}, \dots, C_{66}$  are the elastic moduli that appear in the standard tetragonal elastic tensor [22]. The tetragonal data is estimated for 1480 K in [4]; see also Table II of [11]. The monoclinic data is given in [4]. To allow for a direct comparison with [11], we take the monoclinic data at 1273 K. No experimental data seems to be available for the orthorhombic phase, which is why we fit the orthorhombic data of [9]. Orthorhombic moduli where no data to be fitted are available are marked by ★. Empty entries are zero by symmetry.

The paraboloid can be thought of as a lowest order ansatz to match elastic moduli at one phase, and then modify it continuously along the path so as to match the moduli at the other phases as well. This is along a similar vein to a lowest order polynomial ansatz, but the *sliding* paraboloid does not force us to compromise on the quality of the approximation at some phases. In the examples discussed below, it is immediately obvious that the interpolated paraboloid remains positive definite, while the linear contributions for quadratic invariants are always non-negative. We denote the paraboloid by  $H: \mathbb{R} \rightarrow \mathbb{R}^{(n-1) \times (n-1)}$  with  $H = (h_{jk})_{j,k=1, \dots, n-1}$  and remark that it suffices to choose  $H$  symmetric,  $h_{jk} = h_{kj}$ . The linear contribution is denoted  $\eta: \mathbb{R}^n \rightarrow \mathbb{R}_0^+$ .

The *energy* is then of very simple form, namely

$$\phi(\varrho) := \phi_p(\varrho_0) + \psi(\varrho)^T H(\varrho_0) \psi(\varrho) + \eta(\varrho). \quad (4)$$

We show below that this ansatz gives enough freedom to match the available data for zirconia. The path, the profile and the paraboloid enter as parameters into the fitting process at the phases.

The specific choice of the terms in (4) will be influenced by the requirement that the only global minima of  $\phi$  are at the given phases. Specifically, we ensure that the energy  $\hat{\phi}(\varrho) := \phi_p(\varrho_0) + \psi(\varrho)^T H(\varrho_0) \psi(\varrho)$  without the linear term has no other global minima, which is guaranteed by two observations. On the one hand, we take care that the paraboloid  $H(\varrho_0)$  is always positive definite so that  $\hat{\phi}(\varrho)$  is locally decreasing in at least one direction at any  $\varrho \notin p$ . On the other hand, the path  $p$  itself is constructed in such a way that it only has the three prescribed minima. The linear term  $\eta(\varrho)$  is constructed such that it is non-negative everywhere and vanishes at the three phases. We remark that the linear term deforms the path of lowest energy. Consequently, the path  $p$  alone does not determine the physical transition path and the correction by the linear term has to be taken into account.

### 3.2 Two-dimensional Landau energy for zirconia

In the two-dimensional setting in the  $c_1$ - $c_2$ -plane of Section 2.3.1, the strain variables are  $e_1, e_2$  and  $e_6$ . The position of the three phases with respect to those coordinates is given in Table 1. The invariants (1) then give the location of the phases in the orbit space  $\varrho(\mathbb{R}^3)$ ; see Table 2. Finally, the moduli we want to reproduce are listed in Table 3.

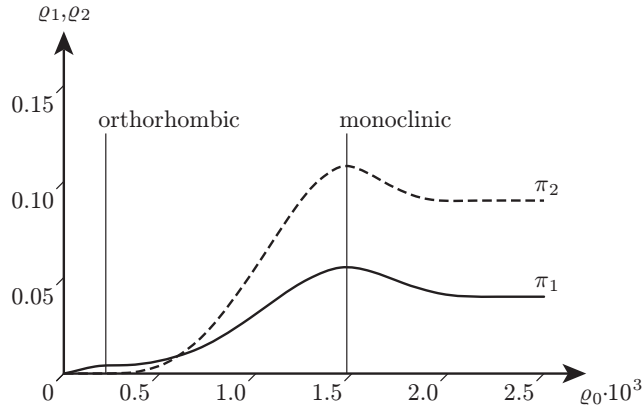


Figure 4: Plots of the path components  $\pi_1$  (solid line) and  $\pi_2$  (dashed line) in the Landau construction.

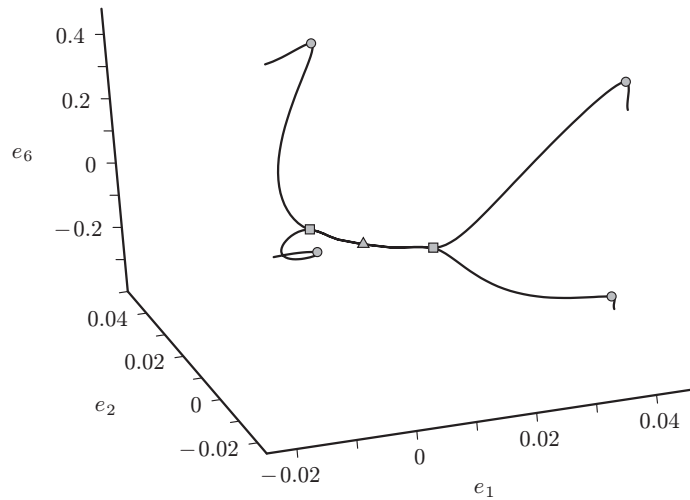


Figure 5: Diagram of the paths in strain space (the image of these paths under  $\varrho$  is the path shown in Figure 4). The paths emerge at the tetragonal phase (triangle) in the origin and remain in the  $e_1$ - $e_2$ -plane before bifurcating at the orthorhombic phases (square) in order to reach the monoclinic phases (circle).

As motivated in Section 3.1, the energy is of the form (4). In particular, the path is parameterised by  $\varrho_0$  and the image of the mapping  $\pi$  has to lie in the half-space  $\{(\varrho_1, \varrho_2) \mid \varrho_2 \geq 0\}$ . We construct both components  $\pi_1$  and  $\pi_2$  as piecewise polynomial functions with two quartic and one quintic segment that join  $C^2$ -continuously at the orthorhombic and the monoclinic phase. Moreover, we constrain the first and second derivatives of the quintic segment to vanish at  $\varrho_0 = \frac{3}{2}\varrho_0^m$  so that it can be continued  $C^2$ -continuously as a constant from there on; see Figure 4. The pre-image of the path in strain space is shown in Figure 5. The profile  $\phi_p$  is defined by five polynomial pieces (quintic, quartic, quartic, quartic, linear) with the same knots as the path plus an additional knot halfway between the orthorhombic and the monoclinic phase that is used to control the height of this saddle; see Figure 6. As for the sliding paraboloid  $H = (h_{jk})_{j,k=1,2}$ , it turns out that it can be modelled by a quadratic function  $h_{11}(\varrho_0)$  and constants  $h_{12}, h_{22}$ . Finally, the linear contribution  $\eta$  is defined as  $\eta(\varrho) := \eta_0(\varrho_0)\varrho_2$ , where  $\eta_0$  is a quartic polynomial between the tetragonal and the monoclinic phase that blends  $C^2$ -continuously into the zero function at the monoclinic phase. The energy in (4) with the prescribed degrees of freedom can then be fitted to exactly match the available data; see Table 4 for the parameters.

	range	$\alpha_0$	$\alpha_1$	$\alpha_2$	$\alpha_3$	$\alpha_4$	$\alpha_5$
$\pi_1$	$[0, r_1]$	0.0	0.0	$4.7022 \cdot 10^5$	$-2.8200 \cdot 10^9$	$4.8117 \cdot 10^{12}$	
	$[r_1, r_2]$	$2.3135 \cdot 10^{-3}$	$1.9044 \cdot 10^1$	$-8.2030 \cdot 10^4$	$1.5114 \cdot 10^8$	$-5.9481 \cdot 10^{10}$	
	$[r_2, r_3]$	-2.9790	$7.0496 \cdot 10^3$	$-6.2815 \cdot 10^6$	$2.6637 \cdot 10^9$	$-5.3184 \cdot 10^{11}$	$3.8974 \cdot 10^{13}$
	$[r_3, \infty)$	0.04					
$\pi_2$	$[0, r_1]$	0.0					
	$[r_1, r_2]$	$-2.5779 \cdot 10^{-3}$	$3.6758 \cdot 10^1$	$-1.8071 \cdot 10^5$	$3.3279 \cdot 10^8$	$-1.3067 \cdot 10^{11}$	
	$[r_2, r_3]$	$-1.4829 \cdot 10^1$	$3.9191 \cdot 10^4$	$-4.0634 \cdot 10^7$	$2.0834 \cdot 10^{10}$	$-5.2925 \cdot 10^{12}$	$5.3360 \cdot 10^{14}$
	$[r_3, \infty)$	0.09					
$\phi_p$	$[0, r_1]$	0.0	$7.6750 \cdot 10^1$	0.0	$-9.2661 \cdot 10^9$	$5.5386 \cdot 10^{13}$	$-9.3070 \cdot 10^{16}$
	$[r_1, r_{1.5}]$	$-3.1271 \cdot 10^{-1}$	$4.6128 \cdot 10^3$	$-2.3951 \cdot 10^7$	$4.9281 \cdot 10^{10}$	$-2.8867 \cdot 10^{13}$	
	$[r_{1.5}, r_2]$	$-5.9011 \cdot 10^1$	$2.1287 \cdot 10^5$	$-2.7033 \cdot 10^8$	$1.4657 \cdot 10^{11}$	$-2.8986 \cdot 10^{13}$	
	$[r_2, r_3]$	$-1.5810 \cdot 10^1$	$3.7594 \cdot 10^4$	$-3.2835 \cdot 10^7$	$1.2391 \cdot 10^{10}$	$-1.6829 \cdot 10^{12}$	
	$[r_3, \infty)$	-2.4932	$1.3545 \cdot 10^3$				
$h_{11}$		$9.3250 \cdot 10^1$	$-1.9951 \cdot 10^4$	$1.2759 \cdot 10^7$			
$h_{12}$		-2.8535					
$h_{22}$		$7.6778 \cdot 10^1$					
$\eta_0$	$[0, r_2]$	$4.7500 \cdot 10^1$	$1.9247 \cdot 10^4$	$-1.7050 \cdot 10^8$	$1.4544 \cdot 10^{11}$	$-3.6269 \cdot 10^{13}$	
	$[r_2, \infty)$	0.0					

Table 4: The coefficients of the parameters for the Landau energy. All functions are polynomials of the form  $\sum_j \alpha_j x^j$ . For those functions which are defined in a piecewise manner, we list the different polynomial segments and indicate the parameter range over which they are defined. Here, the first two knots are the  $\varrho_0$ -coordinates of the orthorhombic and the monoclinic phase,  $r_1 := \varrho_0^o$  and  $r_2 := \varrho_0^m$  (see Table 2), and the third knot is  $r_3 := \frac{3}{2}\varrho_0^m$ . For the profile  $\phi_p$ , we introduce a fourth knot  $r_{1.5} := \frac{1}{2}\varrho_0^o + \frac{1}{2}\varrho_0^m$ . All polynomial pieces join  $C^2$ -continuously at the knots. The data is rounded to the 4th digit.

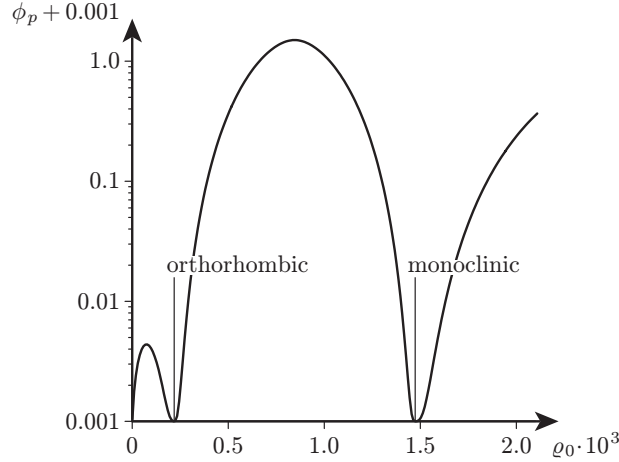


Figure 6: The profile  $\phi_p$  along the path from the tetragonal phase (left, at the origin) via the orthorhombic phase (middle) to the monoclinic phase (right). Since the path is a function of  $\varrho_0 = (e_1 - e_2)^2$ , only non-negative arguments are meaningful.

We call the energy obtained in this way *Landau energy*, since it corresponds to the minimisation of all strain parameters other than the order parameters of the full three-dimensional energy.

We remark that in this framework, it is not hard to check that there are no other local minimisers. To do so, it is not necessary to verify that the gradient of the energy vanishes in the interior of the orbit space (though this is possible here since there are no algebraic dependencies of quantities involved).

	range	$\alpha_0$	$\alpha_1$	$\alpha_2$	$\alpha_3$	$\alpha_4$	$\alpha_5$
$\pi_1$	$[0, r_1]$	0.0	0.0	$1.8977 \cdot 10^5$	$-6.8075 \cdot 10^8$	$8.9528 \cdot 10^{11}$	
	$[r_1, r_2]$	$-1.6530 \cdot 10^{-3}$	$3.2410 \cdot 10^1$	$-4.7474 \cdot 10^4$	$8.8152 \cdot 10^7$	$-3.5987 \cdot 10^{10}$	
	$[r_2, r_3]$	$1.7679 \cdot 10^0$	$-5.9887 \cdot 10^3$	$7.8755 \cdot 10^6$	$-4.9345 \cdot 10^9$	$1.4853 \cdot 10^{12}$	$-1.7313 \cdot 10^{14}$
	$[r_3, \infty)$	0.04					
$\pi_2$	$[0, r_1]$	0.0					
	$[r_1, r_2]$	$-2.5754 \cdot 10^{-3}$	$3.6722 \cdot 10^1$	$-1.8053 \cdot 10^5$	$3.3245 \cdot 10^8$	$-1.3050 \cdot 10^{11}$	
	$[r_2, r_3]$	$-1.4720 \cdot 10^1$	$3.8888 \cdot 10^4$	$-4.0299 \cdot 10^7$	$2.0652 \cdot 10^{10}$	$-5.2436 \cdot 10^{12}$	$5.2841 \cdot 10^{14}$
	$[r_3, \infty)$	0.09					
$\phi_p$	$[0, r_1]$	0.0	$1.3250 \cdot 10^1$	0.0	$-1.6388 \cdot 10^9$	$9.9194 \cdot 10^{12}$	$-1.6886 \cdot 10^{16}$
	$[r_1, r_{1.5}]$	$-3.1916 \cdot 10^{-1}$	$4.6863 \cdot 10^3$	$-2.4226 \cdot 10^7$	$4.9657 \cdot 10^{10}$	$-2.9035 \cdot 10^{13}$	
	$[r_{1.5}, r_2]$	$-5.9131 \cdot 10^1$	$2.1328 \cdot 10^5$	$-2.7084 \cdot 10^8$	$1.4685 \cdot 10^{11}$	$-2.9042 \cdot 10^{13}$	
	$[r_2, r_3]$	$-1.5980 \cdot 10^1$	$3.7967 \cdot 10^4$	$-3.3138 \cdot 10^7$	$1.2497 \cdot 10^{10}$	$-1.6966 \cdot 10^{12}$	
	$[r_3, \infty)$	-2.4993	$1.3572 \cdot 10^3$				
$h_{11}$		$1.3250 \cdot 10^1$	$-2.0969 \cdot 10^4$	$1.2759 \cdot 10^7$			
$h_{12}$		-2.8535					
$h_{22}$		$7.5620 \cdot 10^1$					
$\eta_0$	$[0, r_2]$	$4.7500 \cdot 10^1$	$1.9247 \cdot 10^4$	$-1.7050 \cdot 10^8$	$1.4544 \cdot 10^{11}$	$-3.6269 \cdot 10^{13}$	
	$[r_2, \infty)$	0.0					

Table 5: The coefficients of the parameters for the contribution  $\Phi_{126}$  to the three-dimensional energy. All functions are polynomials of the form  $\sum_j \alpha_j x^j$ . For those functions which are defined in a piecewise manner, we list the different polynomial segments and indicate the parameter range over which they are defined. The four knots  $r_1, r_{1.5}, r_2, r_3$  are the same as in Table 4. All polynomial pieces join  $C^2$ -continuously at the knots. The data is rounded to the 4th digit.

Instead, we can argue in a simple manner, since the energy function is always decreasing in some direction in the interior of  $\varrho(\mathbb{R}^3)$  (except at the global minimisers, which are the t-o-m phases). The same behaviour can be verified for the boundary of the orbit space  $\partial\varrho(\mathbb{R}^3)$  by inspecting the restriction of the energy function to the boundary. The coefficients shown in Table 4 have different orders of magnitude since the input data values (the position of phases and the moduli) differ by orders of magnitude; see Tables 2 and 3. Figure 4 shows that the constructed functions are nevertheless regular, without strong oscillations.

### 3.3 Three-dimensional energy function for zirconia

The two-dimensional construction can be extended to the full three-dimensional setting in a rather straightforward way. We keep the Landau energy of Section 3.2, here denoted  $\Phi_{126}$  to indicate its dependence on  $e_1, e_2$  and  $e_6$ . Since the energetic contributions to be constructed below contribute to the moduli with indices 1, 2 and 6, the parameters of the Landau construction change, and their new values are given in Table 5.

We augment  $\Phi_{126}$  additively by a term  $\Phi_{456}$  in  $e_4, e_5$  and  $e_6$  to fit  $C_{44}, C_{55}$  and  $C_{45}$ . Here, we work in strain space, rather than in orbit space, and employ the invariants  $\varrho_2$  and

$$\begin{aligned}\varrho_8(e_1, \dots, e_6) &:= e_1^2 e_4^2 + e_2^2 e_5^2, \\ \varrho_9(e_1, \dots, e_6) &:= (e_4^2 + e_5^2)(1 + e_6^2) + 4e_4 e_5 e_6.\end{aligned}\tag{5}$$

It is easy to verify that  $\varrho_8 = \varrho_1 \varrho_7 + \frac{1}{4}(\varrho_0 - \varrho_1^2) \varrho_4$  and  $\varrho_9 = (1 + \varrho_2) \varrho_4 + 4\varrho_6$ . The two latter invariants are chosen since they are non-negative. It turns out that the ansatz

$$\Phi_{456} := (a_0 + a_1 \varrho_2) \varrho_4 + b \varrho_8 + c \varrho_9\tag{6}$$

is sufficient to fit the moduli  $C_{44}, C_{45}$  and  $C_{55}$ . This form is considerably simpler than the contributions defined in orbit space, but possible only because so few moduli need to be fitted. Since  $\Phi_{456}$  is

$a_0$	$2.24230 \cdot 10^1$
$a_1$	$5.86247 \cdot 10^1$
$b$	$4.56152 \cdot 10^3$
$c$	$1.05770 \cdot 10^1$

Table 6: The coefficients of the parameters for  $\Phi_{456}$  defined in (6), which constitutes one contribution to the three-dimensional energy. The data is rounded to the 5th digit.

	range	$\alpha_0$	$\alpha_1$	$\alpha_2$	$\alpha_3$	$\alpha_4$	$\alpha_5$	$\alpha_6$
$\pi_1$	$[0, r_1]$	0.0	$3.048 \cdot 10^2$	$-1.459 \cdot 10^6$	$2.324 \cdot 10^9$			
	$[r_1, \infty)$	$2.460 \cdot 10^{-2}$	$-3.294 \cdot 10^1$	$8.656 \cdot 10^4$	$-3.411 \cdot 10^7$			
$\pi_2$	$[0, r_1]$	0.0						
	$[r_1, r_4]$	$-7.825 \cdot 10^{-3}$	$1.172 \cdot 10^2$	$-6.299 \cdot 10^5$	$1.421 \cdot 10^9$	$-1.206 \cdot 10^{12}$	$4.376 \cdot 10^{14}$	$-5.784 \cdot 10^{16}$
	$[r_4, \infty)$	$8.494 \cdot 10^{-2}$						
$\pi_3$	$[0, r_1]$	0.0	$2.285 \cdot 10^2$	$-1.012 \cdot 10^6$	$1.492 \cdot 10^9$			
	$[r_1, \infty)$	$1.538 \cdot 10^{-2}$	$1.732 \cdot 10^1$	$-4.550 \cdot 10^4$	$1.793 \cdot 10^7$			
$\phi_p$	$[0, r_1]$	0.0	$6.350 \cdot 10^1$	0.0	$-7.647 \cdot 10^9$	$4.565 \cdot 10^{13}$	$-7.660 \cdot 10^{16}$	
	$[r_1, r_3]$	$5.511 \cdot 10^{-3}$	$-6.118 \cdot 10^1$	$2.207 \cdot 10^5$	$-2.902 \cdot 10^8$	$1.596 \cdot 10^{11}$	$-3.145 \cdot 10^{13}$	
	$[r_3, \infty)$	$-1.427 \cdot 10^{-3}$	$9.504 \cdot 10^{-1}$					
$h_{11}$		$8.000 \cdot 10^1$	$1.018 \cdot 10^3$					
$h_{13}$		-7.153						
$h_{22}$		1.158						
$h_{33}$		$8.250 \cdot 10^1$	$4.412 \cdot 10^3$					

Table 7: The coefficients of the parameters for the contribution  $\Phi_3$  to the three-dimensional energy. All functions are polynomials of the form  $\sum_j \alpha_j x^j$ . For those functions which are defined in a piecewise manner, we list the different polynomial segments and indicate the parameter range over which they are defined. The knots are  $r_1 := \varrho_0^o$ ,  $r_2 := \varrho_0^m$  (see Table 2),  $r_3 := 1.554 \cdot 10^{-3}$  and  $r_4 := 2.210 \cdot 10^{-3}$ . All polynomial pieces join  $C^2$ -continuously at the knots. The data is rounded to the 3rd digit.

non-negative, it is easy to verify that minima exist only at the tetragonal, the orthorhombic and the monoclinic phase. The parameters for  $\Phi_{456}$  are given in Table 6.

To match the elastic moduli involving the strain component  $e_3$ , we employ the path-profile construction with the four invariants  $\tilde{\varrho}_0 := \varrho_0$ ,  $\tilde{\varrho}_1 := \varrho_1 + \varrho_3$ ,  $\tilde{\varrho}_2 := \varrho_2$ ,  $\tilde{\varrho}_3 := \varrho_3$ . Again, we choose the invariant  $\tilde{\varrho}_0$  for the parameterisation of the path, the profile and the sliding paraboloid. As for the latter, it turns out that it suffices to involve only  $h_{11}$ ,  $h_{22}$ ,  $h_{13}$  and  $h_{33}$ , and set the other components to zero. Moreover, the linear contribution  $\eta$  is not needed for this energetic contribution that we denote  $\Phi_3$ ; see Table 7 for details.

An energy that fits exactly all available moduli is then

$$\Phi := \Phi_{126} + \Phi_{456} + \Phi_3, \quad (7)$$

considered as a function in strain space, that is, the invariants are evaluated with the strain variables.

An examination of the energy reveals that no global minimisers other than the prescribed ones exist. Local minimisers could in principle exist due to the addition of three energetic terms, because gradients could cancel out locally. An analysis of the saddle point via Newton search as in [16] could be employed to examine the existence of local minima.

## 4 Physical interpretation and numerical illustration

One key feature of the approach advocated here is that it allows the modelling of the lowest energy path between stable phases. The conventional polynomial expansion is less suitable for the description of this transition path. This is because a polynomial interpolation of several points already leads in

normal circumstances to significant oscillations, while no such oscillations are expected for a macroscopic energy density. Since we propose a method that can model the energy along this low-energy transition path with arbitrary precision, the question arises as to how this path can be determined for arbitrary phase-transforming materials. One suitable method would be an *ab initio* calculation, where a sufficiently large region in the strain space is explored. Such a sequence of simulations would in principle determine the path and the elastic moduli along the path, though the detection of this path in higher space dimensions is far from trivial. Alternatively, an experiment where a specimen is exposed to forces that trigger a transformation along the path can then be used to determine the moduli experimentally. The high temperature and pressure of the triple point, however, pose a serious challenge for such a sophisticated experiment, and we are not aware of such data. The available measurements for the elastic moduli of the stable phases already have significant error margins, in particular for the off-diagonal moduli; the problem of precise measurements would be significantly accentuated for the sequence of out-of-equilibrium measurements of the moduli along the transition path. In principle, however, such experiments are possible since a suitable load transforms a point on the transition path into an equilibrium configuration.

The energy barriers along the path influence various physical quantities. For example, the transformation stress (i.e., the stress required to trigger a stress-induced transformation) depends on the height of the profile. The reason is that the energy barrier defined by the profile is on the mountain pass connection between minima, and a mountain pass connection is the energetically most favourable connection. The height  $h$  of the mountain pass is a function of the energy barrier and the applied stress. For example, for a spring-chain model, it can be shown rigorously [24] that the transition is given by the mountain pass, even if there are many possible ways to transform from one metastable state to another.

We restrict the analysis here to the isothermal situation; the inclusion of thermal effects is discussed elsewhere [16]. In [16], the focus is on the influence of stress on the transformation temperature via the Clausius-Clapeyron equation. We mention here that the energy barriers influence the dependence of the specific heat on the temperature. For first order phase transitions, the temperature dependence of the specific heat exhibits a sharp peak around the transformation temperature due to the presence of latent heat. The latent heat released during the transformation is given by the area enclosed by the hysteresis loop of the transformation; this area in turn depends on the transformation strain.

While experiments at the high temperature and pressure of the triple point are very difficult, numerical simulations offer the possibility to analyse the formation of microstructures in this regime of particular interest.

One question of interest is the propagation of a phase front. In the static situation, one would expect different effects to compete against each other. Namely, on the one hand the transition path constructed here is the energetically favourable path for the transformation of one phase into another. On the other hand, if the two phases form a sharp interface, then this imposes a constraint since the displacement has to be continuous across the interface. It is well known that this constraint can be expressed as the condition that the strain gradients of the two phases,  $A$  and  $B$ , say, are connected by a rank-one line,  $A - B = a \otimes b$  with  $a, b \in \mathbb{R}^n$  [1], here with  $n = 2$  or  $n = 3$ . Thus, there is competition between the energetically favourable transformation path and a transition along a rank-one line that connects two phases. We investigate this competition in the presence of dynamics and interfacial energy. Specifically, we employ the finite element method to study the behaviour of a system consisting of the Landau energy, a higher gradient surface energy term, and the kinetic energy. We also add a viscosity term to slowly relax the system to a stationary point. This leads to the equation of motion

$$\ddot{u} = \text{Div } \sigma - \gamma \Delta^2 u + \beta \Delta \dot{u}$$

for the displacement  $u = u(x, t)$ , with coefficients  $\gamma$  and  $\beta$  controlling the surface energy and viscosity, respectively. The divergence of the stress  $\sigma = \frac{\partial \Phi(F)}{\partial F}$  is taken row-wise.

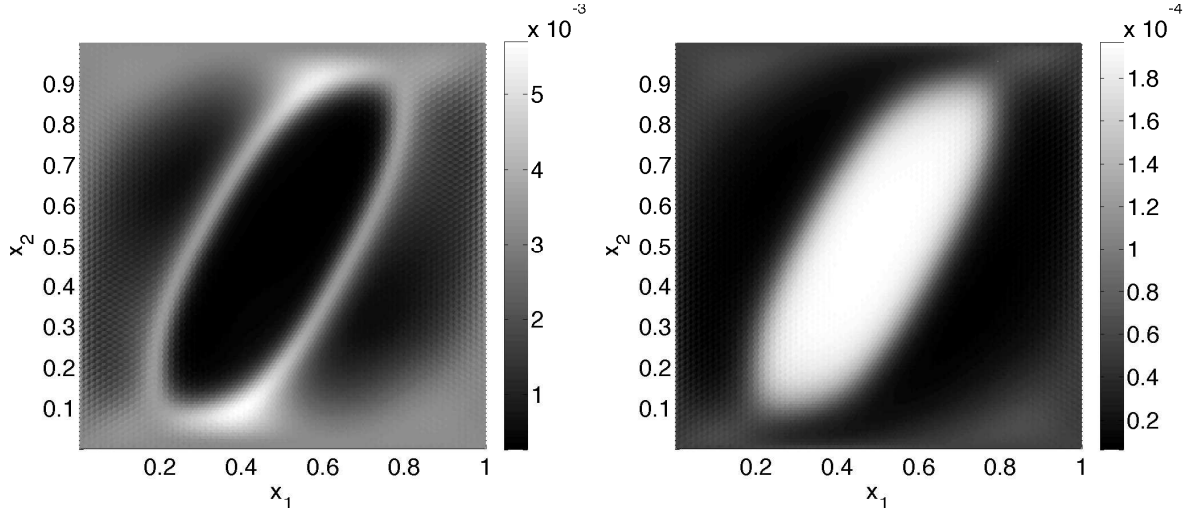


Figure 7: Results of the simulation for a tetragonal-orthorhombic phase boundary. Initial values and boundary values are on a rank 1 connection in between the two minima. The left panel shows the elastic energy density  $\Phi(\varrho(x))$ , the right panel shows the clear distinction between the two phases in the order parameter  $\varrho_0$ .

#### 4.1 Numerical solution method

We use a finite element discretisation with basis functions derived from Loop subdivision surfaces, which can be thought of as a generalisation of multivariate splines to tessellations of arbitrary topology [21]. We resort to such a discretisation of  $C^1$ -smoothness to correctly evaluate the strain gradient energy terms, which contain higher order derivatives. The use of subdivision surfaces for this problem has been suggested in [6]. The simulation employed is very similar to the one used in [8] and more information on the method can be found there. We do, however, use the method described in [2] to fix the clamped boundary conditions (i.e., Dirichlet and natural Neumann boundary data for the 4th order initial-boundary value problem). A constant affine tilt  $F_{\text{tilt}}$  is added to the gradient of  $u$  in the computation to achieve non-zero boundary conditions. In order to advance the system in time, we use an explicit Newmark scheme. The computational domain is a square of size 1, discretised with 28 293 triangular elements using `distmesh` [23].

#### 4.2 Computational results

Figure 7 shows the relaxed state of a simulation with tilt

$$F_{\text{tilt}}^{\text{t-o}} = \begin{pmatrix} 4.6608 & -3.5505 \\ 3.5505 & -2.7154 \end{pmatrix} \cdot 10^{-3} \quad \text{and} \quad \gamma = 0.4, \quad \beta = 0.1.$$

This tilt has been chosen since it is located on a rank-1-connection, exactly half way between a tetragonal and an orthorhombic minimum. Therefore, the microstructure displayed in Figure 7, alternating between the two minima, develops. As expected, the lamination occurs approximately across the habit plane of the system.

Since the main thrust of this article is the derivation of an explicit expression of the potential energy at the triple point, we contrast the numerical findings with those for the setting where the potential energy is given as a lowest-order polynomial expansion. Figure 8 displays the result of a simulation with the energy presented here replaced by the conventional polynomial Landau expansion. The parameters in this simulation are

$$F_{\text{tilt}}^{\text{t-o}} = \begin{pmatrix} 3.5768 & 3.6027 \\ -3.6027 & -3.6287 \end{pmatrix} \cdot 10^{-3} \quad \text{and} \quad \gamma = 0.4, \quad \beta = 0.1.$$

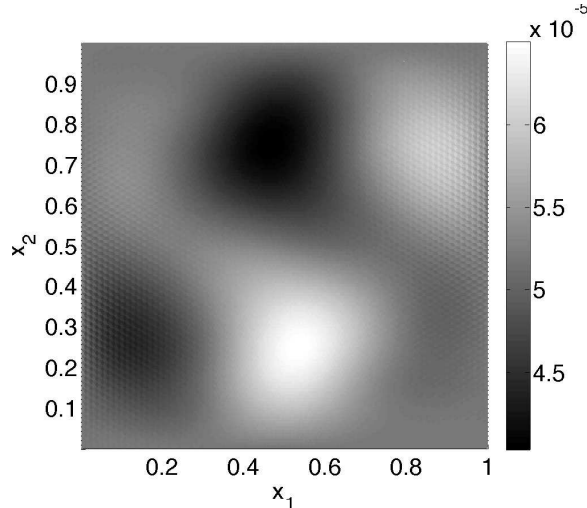


Figure 8: Simulation using the same parameters as in Figure 7, but employing the polynomial energy landscape from [11]. Shown is the order parameter  $\varrho_0$ , as in Figure 7 (right). No clear distinction between the phases can be observed (note that the scaling of the order parameter is  $10^{-5}$ , so the variation is two orders of magnitude smaller).

We take the energy from [11], restricted to the  $e_1$ - $e_2$ - $e_6$ -plane and evaluated at the triple point temperature (840 K) and pressure (1.8 GPa). This energy uses a slightly different two-dimensional reduction of the system, therefore the minima are at slightly different positions. Again, there is a mountain pass, that is, a transformation path. It turns out that the energy is essentially flat along the path between the minima, with an extremely low energy barrier. In other words, the conventional polynomial expansion yields an unrealistic estimate of the energy barrier, unlike the method presented here. Consequently, for this polynomial energy, there is no clear distinction between the orthorhombic and the tetragonal phase in the simulation, even though the affine tilt was again chosen to be exactly half-way in between the tetragonal and an orthorhombic minimum on a rank-one connection. The surface energy and the viscosity are the same as in the previous simulation. The simulation result is shown in Figure 8. The two phases in the polynomial energy would lie at  $\varrho_0 = 0.0$  (tetragonal) and  $\varrho_0 = 2.0767 \cdot 10^{-4}$  (orthorhombic), respectively.

In Figure 9, the relaxed state of a simulation with tilt

$$F_{\text{tilt}}^{\text{t-m}} = \begin{pmatrix} 1.0110 \cdot 10^{-2} & -1.6135 \cdot 10^{-1} \\ -6.0095 \cdot 10^{-4} & -8.8811 \cdot 10^{-3} \end{pmatrix} \quad \text{and} \quad \gamma = 0.4, \quad \beta = 0.1.$$

is presented. The value for  $F_{\text{tilt}}^{\text{t-m}}$  lies exactly half way between a tetragonal and a monoclinic minimum on a rank 1 connection between the two. The arrangement of phases in the resulting picture is complex, due to a strong influence of the boundary. One can observe, however, that there are separate regions where the strain is close to the tetragonal or orthorhombic phase and close to the monoclinic phase, respectively.

These results show that the energy landscape constructed here is very well suited for use in finite element codes.

## 5 Discussion

With regard both to the theory and applications of solid phase transitions, there is a general interest in devising a methodology that allows for the integration of experimental data for multiphase materials into an energy density via a straightforward and phenomenological, yet natural approach. Here, we

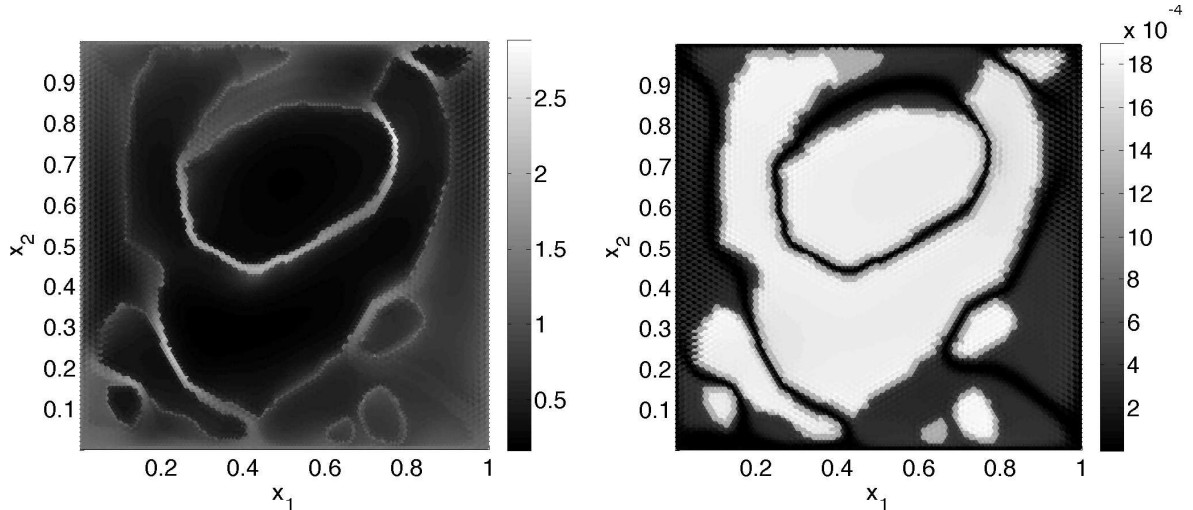


Figure 9: Elastic energy density (left) and order parameter  $\rho_0$  (right) of the fully relaxed state of a simulation with initial and boundary conditions on a rank 1 connection in between the tetragonal and the monoclinic minima of the energy. A complex arrangement of phases has formed, with boundaries of higher energy in between.

propose the *path-profile construction*. The intuition behind this method is the observation that a good phenomenological description of the energy landscape needs to describe the local properties of the stable phases correctly, and has to offer a phenomenologically appropriate transformation path. The classical approach with invariant polynomials is well suited for the former, but not for the latter. We develop a method to model a phenomenological transformation path such that local properties can be fitted with relative ease. The approach has recently been used in a less explicit fashion to model one contribution to an energy for InTl [16]. Here, we demonstrate the simplicity of the method by choosing a material with a triple point. We first derive the Landau contribution, which only relies on order parameters, and apply the path-profile construction. The energy as a function of the three-dimensional strain tensor is then obtained via extension.

The approach proposed here is general, even if the specific examples are genuine for zirconia. We noticed that the process of fitting is remarkably easy, since the construction with the sliding paraboloid greatly facilitates the process. The calculations for the fitting process were done in Maple, where a straightforward implementation requires at most a few seconds to complete on a personal computer.

It is possible to construct the energy entirely in the orbit space, rather than composing it from three different terms, as is the case here. Although the approach to work in the full orbit space may be more elegant and ultimately more straightforward, some technical aspects remain to be overcome. Namely, it becomes more difficult to rule out minima on the boundary. This matter will be the topic of a future investigation. Also, it is not evident which set of invariants should be chosen. In the low-dimensional approach, as advocated here, it is easy to test and compare different choices, while the analogous procedure becomes much more involved when the number of invariants involved is increased.

It has been noted that using a lowest-order polynomial as the Gibbs energy density necessarily introduces a second orthorhombic phase for which experimental evidence seems to be unavailable [11]. While this phase is stable at zero pressure only for a small range of temperatures above 1520 K and becomes unstable for pressure over 1.35 GPa [11], it has been shown to be the most stable phase for the polynomial energy under various shear loads at room conditions [12]. Since the existence of this phase may have implications on zirconia as a toughening agent near crack tips, it seems desirable to examine whether other energy densities also predict this phase. The present isothermal energy density may serve as a basis for such investigations.

## Acknowledgements

The Interactive Ideas Factory at the University of Bath, an EPSRC Bridging the Gaps project (EP/E018122/1) funded a visit of J. Z. to Clausthal University of Technology, during which most of the work reported here was carried out. J. Z. gratefully acknowledges the financial support of the EPSRC through an Advanced Research Fellowship (GR/S99037/1). We thank Chris Bowen, Kaushik Dayal, Peter Schröder, and Heinrich-Gregor Zirnstein for helpful comments.

## References

- [1] K. Bhattacharya. *Microstructure of Martensite. Why it forms and how it gives rise to the shape-memory effect.*, volume 2 of *Oxford Series on Materials Modelling*. Oxford University Press, New York, 2003.
- [2] H. Biermann, A. Levin, and D. Zorin. Piecewise smooth subdivision surfaces with normal control. In *Proceedings of SIGGRAPH 2000*, pages 113–120, New Orleans, July 2000. ACM Press.
- [3] S.-K. Chan. The polymorphic transformations of zirconia. *Physica B+C*, 150(1–2):212–222, May 1988.
- [4] S.-K. Chan, Y. Fang, M. Grimsditch, Z. Li, M. V. Nevitt, W. M. Robertson, and E. S. Zouboulis. Temperature-dependence of the elastic moduli of monoclinic zirconia. *Journal of the American Ceramic Society*, 74(7):1742–1744, July 1991.
- [5] C. Chevalley. Invariants of finite groups generated by reflections. *American Journal of Mathematics*, 77(4):778–782, Oct. 1955.
- [6] F. Cirak, M. Ortiz, and P. Schröder. Subdivision surfaces: A new paradigm for thin-shell finite-element analysis. *International Journal for Numerical Methods in Engineering*, 47(12):2039–2072, Apr. 2000.
- [7] C. S. G. Cousins. The symmetry of inner elastic constants. *Journal of Physics C: Solid State Physics*, 11(24):4881–4900, Dec. 1978.
- [8] P. W. Dondl, C.-P. Shen, and K. Bhattacharya. Computational analysis of martensitic thin films using subdivision surfaces. *International Journal for Numerical Methods in Engineering*, 72(1):72–94, Oct. 2007.
- [9] P. W. Dondl and J. Zimmer. Modeling and simulation of martensitic phase transitions with a triple point. *Journal of the Mechanics and Physics of Solids*, 52(9):2057–2077, Sept. 2004.
- [10] J. L. Ericksen. Some phase transitions in crystals. *Archive for Rational Mechanics and Analysis*, 73(2):99–124, June 1980.
- [11] G. Fadda, L. Truskinovsky, and G. Zanzotto. Unified Landau description of the tetragonal, orthorhombic, and monoclinic phases of zirconia. *Physical Review B*, 66(17):174107, Nov. 2002.
- [12] G. Fadda, L. Truskinovsky, and G. Zanzotto. Nonhydrostatic stabilization of an orthorhombic phase of zirconia. *Physical Review B*, 68(13):134106, Oct. 2003.
- [13] F. Falk and P. Konopka. Three-dimensional Landau theory describing the martensitic phase transformation of shape-memory alloys. *Journal of Physics: Condensed Matter*, 2(1):61–77, Jan. 1990.
- [14] R. J. Gooding, Y. Y. Ye, C. T. Chan, K.-M. Ho, and B. N. Harmon. Role of non-symmetry-breaking order parameters in determining the martensitic energy barrier: The bcc-to-9R transformation. *Physical Review B*, 43(16):13626–13629, June 1991.

- [15] G.-M. Greuel, G. Pfister, and H. Schönemann. SINGULAR 2.0. A computer algebra system for polynomial computations, Centre for Computer Algebra, University of Kaiserslautern, 2001. <http://www.singular.uni-kl.de>.
- [16] K. Hormann and J. Zimmer. On Landau theory and symmetric energy landscapes for phase transitions. *Journal of the Mechanics and Physics of Solids*, 55(7):1385–1409, July 2007.
- [17] Y. Huo and I. Müller. Interfacial and inhomogeneity penalties in phase transitions. *Continuum Mechanics and Thermodynamics*, 15(4):395–407, Aug. 2003.
- [18] R. D. James. Unpublished notes. Private communication, 1988.
- [19] A. Kuwabara, T. Tohei, T. Yamamoto, and I. Tanaka. *Ab initio* lattice dynamics and phase transformations of  $\text{ZrO}_2$ . *Physical Review B*, 71(6):064301, Feb. 2005.
- [20] L. D. Landau. On the theory of phase transitions. In D. ter Haar, editor, *Collected papers of L. D. Landau*. Gordon & Breach, New York, 1965.
- [21] C. T. Loop. Smooth subdivision surfaces based on triangles. Master’s thesis, Department of Mathematics, University of Utah, Aug. 1987.
- [22] A. E. H. Love. *A Treatise on the Mathematical Theory of Elasticity*. Dover, New York, fourth edition, 1944.
- [23] P.-O. Persson and G. Strang. A simple mesh generator in MATLAB. *SIAM Review*, 46(2):329–345, June 2004.
- [24] G. Puglisi and L. Truskinovsky. Rate independent hysteresis in a bi-stable chain. *Journal of the Mechanics and Physics of Solids*, 50(2):165–187, Feb. 2002.
- [25] N. Simha and L. Truskinovsky. Shear induced transformation toughening in ceramics. *Acta Metallurgica et Materialia*, 42(11):3827–3836, Nov. 1994.
- [26] G. F. Smith and R. S. Rivlin. The strain-energy function for anisotropic elastic materials. *Transactions of the American Mathematical Society*, 88(1):175–193, May 1958.
- [27] L. Truskinovsky and G. Zanzotto. Elastic crystals with a triple point. *Journal of the Mechanics and Physics of Solids*, 50(2):189–215, Feb. 2002.
- [28] H. Weyl. *The Classical Groups: Their Invariants and Representations*. Princeton Landmarks in Mathematics and Physics. Princeton University Press, Princeton, NJ, second edition, 1997. Fifteenth printing.
- [29] J. Zimmer. Stored energy functions for phase transitions in crystals. *Archive for Rational Mechanics and Analysis*, 172(2):191–212, May 2004.